Fast binomial-code holonomic quantum computation with ultrastrong light-matter coupling

Ye-Hong Chen [1], Wei Qin [1,*], Roberto Stassi [1,2], Xin Wang [1,3] and Franco Nori [1,4,5,†]

[1]*Theoretical Quantum Physics Laboratory, RIKEN Cluster for Pioneering Research, Wako-shi, Saitama 351-0198, Japan*
[2]*Dipartimento di Scienze Matematiche e Informatiche, Scienze Fisiche e Scienze della Terra, Università di Messina, 98166, Messina, Italy*
[3]*Institute of Quantum Optics and Quantum Information, School of Science, Xi'an Jiaotong University, Xi'an 710049, China*
[4]*Department of Physics, University of Michigan, Ann Arbor, Michigan 48109-1040, USA*
[5]*RIKEN Center for Quantum Computing (RQC), Wako-shi, Saitama 351-0198, Japan*

(Received 18 December 2020; accepted 31 August 2021; published 24 September 2021)

We propose a protocol for bosonic binomial-code nonadiabatic holonomic quantum computation in a system composed of an artificial atom ultrastrongly coupled to a cavity resonator. In our protocol, the binomial codes, formed by superpositions of Fock states, can greatly save physical resources to correct errors in quantum computation. We apply to the system strong driving fields designed by shortcuts-to-adiabatic methods. This reduces the gate time to *tens of nanoseconds*. Noise induced by control imperfections can be suppressed by a systematic-error-sensitivity nullification method. As a result, this protocol can rapidly ($\sim$35 ns) generate fault-tolerant and high-fidelity ($\gtrsim$98% with experimentally realistic parameters) quantum gates.

DOI: 10.1103/PhysRevResearch.3.033275

I. INTRODUCTION

The generation of robust and fault-tolerant quantum gates is a basic requirement for quantum computation. To reach this goal, much attention has been given to holonomic quantum computation [1–4] based on Abelian [5,6] and non-Abelian geometric phases [7–9]. These can provide a robust way towards universal quantum computation, because the geometric phases are determined by the global properties of the evolution paths and possess a built-in noise-resilience feature against certain types of local noises [10–13]. In particular, nonadiabatic holonomic quantum computation (NHQC) [14–20] releases the variations of parameters from the limitation of the adiabatic condition, making the computation fast and robust against local parameter fluctuations over the cyclic evolution. However, due to the huge physical resource overhead and the difficulties in scaling up the number of qubits [21–31], previous work [2–4,14–20,32–42] showed that is experimentally difficult to implement a quantum error-correction protocol [25,43–45] in NHQC. For this reason, holonomic computation via bosonic codes [46,47] has attracted much interest recently [48,49]. Bosonic codes allow quantum error correction extending only the number of excitation instead of the number of qubits, while keeping the noise channels fixed [48–64]. For instance, binomial codes [54] formed from superposition of Fock states are protected against continuous dissipative evolution under loss, gain, and dephasing errors.

Unfortunately, universal control of a single bosonic mode is difficult due to its harmonicity. Although adding direct and indirect nonlinear interactions can induce weak anharmonicity [53], it is still difficult to manipulate independently and simultaneously every needed Fock state. Moreover, weak nonlinear interactions may induce additional noises into the system and limit the gate fidelities [53]. This, with additional operations (e.g., feedback [60,65,66] and driven-dissipative controls [48,51]) and conditions (e.g., oscillators and qubits are never driven simultaneously [55,67,68]), makes it difficult to implement NHQC [14,17,18] with bosonic error-correction codes. Note that the first experiment for binomial-code conditional geometric gates was recently realized [55] using three-dimensional (3D) superconducting cavities, but it is not a holonomic computation.

The eigenstates of a two-level atom and a cavity field interacting in the ultrastrong coupling (USC) regime are anharmonic dressed atom-light states [69–88]. In this manuscript, to overcome the problems mentioned in the previous paragraph, we use these dressed states as intermediate states [89–94] to simultaneously couple a different Fock basis and induce population transitions between them. To implement NHQC with binomial codes, we populate Fock states in one step, driving the atom with a composite pulse. The strong anharmonicity in the USC regime allows one to apply strong driving fields [91–93] in order to shorten the gate time to nanoseconds. These drives are designed by an invariant-based method [95–101] and a systematic-error-sensitivity nullification method [18,19,102], making our protocol fast and robust against pulse imperfections. Additionally, the NHQC protocol presented here is scalable for multiqubit gates ultrastrongly coupling the atom to a multimode cavity.

*wei.qin@riken.jp
†fnori@riken.jp

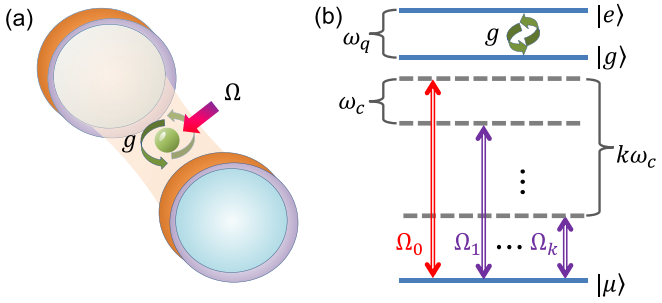

FIG. 1. (a) Schematic illustration of an atom-cavity combined system. (b) Level diagram of the bare three-level atom. The upper two levels ($|e\rangle$, $|g\rangle$) of the atom are ultrastrongly coupled to the cavity mode with strength g. The lower two levels ($|g\rangle$, $|\mu\rangle$) are off-resonantly driven by a composite pulse $\Omega = \sum_k \Omega_k \cos(\omega_k t + \phi_k)$.

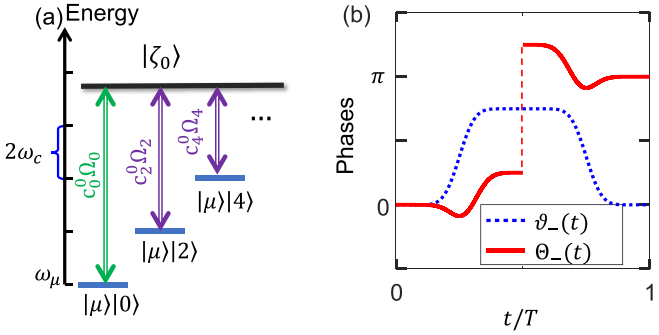

FIG. 2. (a) Illustration of the effective transitions according to Eq. (6). (b) Dynamical and geometric phases acquired by the evolution along $|\psi_-(t)\rangle$ with parameters given in Eq. (19) and $\Theta_s = \pi/2$.

II. MODEL AND EFFECTIVE HAMILTONIAN

Our system consists of a three-level ($|e\rangle$, $|g\rangle$, $|\mu\rangle$) artificial atom and a cavity resonator [103]. The states $|e\rangle$ and $|g\rangle$ are ultrastrongly coupled to a cavity mode [104], with coupling strength g (see Fig. 1). The atom-cavity interaction is described by $H_0 = H_R + \hbar\omega_\mu|\mu\rangle\langle\mu|$, where

$$H_R = \hbar\omega_c a^\dagger a + \frac{\hbar\omega_q}{2}\sigma_g^z + \hbar g(a + a^\dagger)\sigma_g^x \tag{1}$$

is the Rabi Hamiltonian. Here, $\sigma_g^x = |e\rangle\langle g| + |g\rangle\langle e|$ and $\sigma_g^z = |e\rangle\langle e| - |g\rangle\langle g|$ are Pauli matrices, a ($a^\dagger$) is the annihilation (creation) operator of the cavity field, ω_μ is the frequency of the level $|\mu\rangle$, and $\omega_{c,(q)}$ is the cavity (qubit) frequency. In the USC regime ($g/\omega_c \gtrsim 0.1$), the eigenstates $|\mathcal{E}_j\rangle$ with eigenvalues ξ_j of H_0 can be separated into (i) noninteracting sectors $|\mu\rangle|n\rangle$ with eigenvalues $\omega_\mu + n\omega_c$ and (ii) dressed atom-cavity states $|\zeta_m\rangle$ with eigenvalues E_m ($j, n, m = 0, 1, 2, \ldots$). Here, $|n\rangle$ denotes the Fock states of the cavity mode, and

$$|\zeta_m\rangle = \sum_n \left(c_n^m|g\rangle|n\rangle + d_{n\pm1}^m|e\rangle|n \pm 1\rangle\right) \tag{2}$$

denotes the dressed states of H_R. The coefficients $c_n^m = \langle\zeta_m|g\rangle|n\rangle$ and $d_{n\pm1}^m = \langle\zeta_m|e\rangle|n \pm 1\rangle$ can be obtained numerically. Note that we impose $d_{-1}^m = 0$ for Eq. (2).

Oscillations $|\mu\rangle|n\rangle \leftrightarrow |\zeta_m\rangle$ can be induced by driving the atomic transition $|\mu\rangle \leftrightarrow |g\rangle$ [see Fig. 1(b)] with an additional control Hamiltonian:

$$H_D(t) = \hbar\Omega(|\mu\rangle\langle g| + |g\rangle\langle\mu|). \tag{3}$$

Here,

$$\Omega = \sum_k \Omega_k \cos(\omega_k t + \phi_k) \tag{4}$$

is a composite pulse [65,91,105,106] with amplitudes Ω_k, frequencies ω_k, and phases ϕ_k. We omit the explicit time dependence of all the parameters (e.g., Ω_k and ϕ_k) regarding the drivings. The total Hamiltonian is $H_{\rm tot}(t) = H_0 + H_D(t)$. Choosing

$$\begin{aligned} &\omega_k = (E_m - \omega_\mu - k\omega_c) \\ &\Omega_k \ll \omega_c, g, \end{aligned} \tag{5}$$

and performing a unitary transformation $\exp(-iH_0 t)$, we derive an effective Hamiltonian that, under the rotating wave approximation, is (see details in Appendix A)

$$H_{\rm eff}(t) = \frac{\hbar}{2}\sum_{k=0}^{k_{\max}} c_k^m \Omega_k e^{i\phi_k}|\mu\rangle|k\rangle\langle\zeta_m| + \text{H.c.} \tag{6}$$

This effective Hamiltonian describes transitions between the Fock states $|k\rangle$ through the dressed intermediate state $|\zeta_m\rangle$. We assume

$$\omega_\mu = E_m - (k_{\max} + 0.25)\omega_c, \tag{7}$$

so that the dressed state $|\zeta_m\rangle$ is the highest level in the evolution subspace. In Fig. 2(a) we illustrate the effective transitions for $m = 0$. Note that each Fock state can be freely populated by the drivings Ω_k when the system is in the USC regime. Instead, in the weak-coupling regime, the qubit driving $H_D(t)$ only induces oscillations $|g\rangle|0\rangle \leftrightarrow |\mu\rangle|0\rangle$ because $c_{n\neq0}^{m=0} \simeq 0$.

III. NONADIABATIC HOLONOMIC QUANTUM COMPUTATION VIA BINOMIAL CODES

An example of the binomial codes [54] for single-qubit gates protecting against the single-photon loss error is

$$|\tilde{1}\rangle = |2\rangle, \quad |\tilde{0}\rangle = (|0\rangle + |4\rangle)/\sqrt{2}, \tag{8}$$

which form a computational subspace $\mathcal{S}_c = \{|\tilde{0}\rangle, |\tilde{1}\rangle\}$. With this definition, a photon loss error brings the logical code words to a subspace with odd photon numbers that is clearly disjoint from the even-parity subspace of the logical code words [54]. The Knill-Laflamme condition [107,108] for this kind of codes reads $\langle\tilde{\varrho}|a^\dagger a|\tilde{\varrho}'\rangle = 2$ ($\varrho, \varrho' = 0, 1$). This means that the probability of a photon jump to occur is the same for $|\tilde{0}\rangle$ and $|\tilde{1}\rangle$, implying that the quantum state is not deformed under the error of a photon loss. For instance, when encoding quantum information as

$$|\psi_0\rangle = \cos\chi|\tilde{0}\rangle + \sin\chi|\tilde{1}\rangle, \tag{9}$$

a photon jump leads to

$$|\psi_1\rangle = \frac{a|\psi_0\rangle}{\sqrt{\langle\psi_0|a^\dagger a|\psi_0\rangle}} = \cos\chi|3\rangle + \sin\chi|1\rangle, \tag{10}$$

which means that the information ($\cos\chi$ and $\sin\chi$) is not deformed [54].

To manipulate the codes in Eq. (8), we need a three-frequency composite pulse, i.e., $k = (0, 2, 4)$ in Eq. (6). When $g/\omega_c \gtrsim 0.5$, the probability amplitudes (c_0^2, c_2^2, c_4^2) of the Fock states $(|0\rangle, |2\rangle, |4\rangle)$ in the third dressed state $|\zeta_2\rangle$ are greater than in the other dressed states (see more details in Appendix A). For this reason, we choose $m = 2$ in Eq. (6). Assuming $c_0^2\Omega_0 = c_4^2\Omega_4$ and $\phi_0 = \phi_4$, $H_{\rm eff}(t)$ becomes an effective Λ-type system with two ground states $\{|\tilde{0}\rangle, |\tilde{1}\rangle\}$ and an excited state $|\zeta_2\rangle \equiv |\zeta_{m=2}\rangle$. The NHQC in a Λ-type system has been well studied [3,4,11]. For clarity, we define an effective driving amplitude,

$$\Xi = \sqrt{\sum_k \left(c_k^2\Omega_k\right)^2}, \tag{11}$$

and a time-independent parameter,

$$\theta = \frac{1}{2}\arctan\left(\frac{\sqrt{2}c_0^2\Omega_0}{c_2^2\Omega_2}\right), \tag{12}$$

to rewrite $H_{\rm eff}(t)$ to be

$$H_{\rm eff}(t) = \frac{\hbar}{2}\Xi\exp(i\phi_2)|b\rangle\langle\zeta_2| + \text{H.c.}, \tag{13}$$

where $\phi = \phi_2 - \phi_0$ and

$$|b\rangle = e^{-i\phi}\sin(\theta/2)|\tilde{0}\rangle|\mu\rangle + \cos(\theta/2)|\tilde{1}\rangle|\mu\rangle. \tag{14}$$

Initially, quantum information is stored in the logical qubit states of the subspace $\mathcal{S}_c$ (the atom is in $|\mu\rangle$). According to the invariant-based approaches for Λ-type transitions [100,101,109], when

$$\begin{aligned}\Xi\sin\phi_2 &= \Omega_p(\beta,\varphi) \equiv (\dot\beta\cot\varphi\sin\beta + \dot\varphi\cos\beta),\\ \Xi\cos\phi_2 &= \Omega_s(\beta,\varphi) \equiv (\dot\beta\cot\varphi\cos\beta - \dot\varphi\sin\beta),\end{aligned} \tag{15}$$

the Hamiltonian in Eq. (13) can drive the system to evolve exactly along one of the two user-defined paths (see details in Appendix B):

$$\begin{aligned}|\psi_+(t)\rangle &= \sin(\varphi/2)|\mu\rangle|b\rangle + i\exp(i\beta)\cos(\varphi/2)|\zeta_2\rangle,\\ |\psi_-(t)\rangle &= i\exp(i\beta)\cos(\varphi/2)|b\rangle + \sin(\varphi/2)|\zeta_2\rangle,\end{aligned} \tag{16}$$

which are two eigenstates of a dynamical invariant $I(t)$ obeying $\hbar\partial_t I(t) = i[H_{\rm eff}(t), I(t)]$. For instance, when $\varphi(0) = 0$, the evolution is along $|\psi_-(t)\rangle$, which acquires a dynamical phase,

$$\vartheta_-(t) = -\frac{1}{\hbar}\int_0^t \langle\psi_-(t')|H_{\rm eff}(t')|\psi_-(t')\rangle dt', \tag{17}$$

and a geometric phase,

$$\Theta_-(t) = \int_0^t \langle\psi_-(t')|i\partial_{t'}|\psi_-(t')\rangle dt'. \tag{18}$$

For a cyclic evolution, the time-dependent auxiliary parameters β and φ need to satisfy $\beta(0) \neq \beta(t_f)$ and $\varphi(0) = \varphi(t_f) = 0$. We can choose

$$\begin{aligned}\varphi &= \pi\sin^2(\pi t/T),\\ \beta &= \frac{2}{3}\begin{cases}2\sin^3\varphi, & t\in[0, t_f/2]\\ 2\sin^3\varphi - 3\Theta_s. & t\in[t_f/2, t_f].\end{cases}\end{aligned} \tag{19}$$

Thus the final phases are $\vartheta_-(t_f) = 0$ and $\Theta_-(t_f) = 2\Theta_s$ [see Fig. 2(b) and Appendix B], resulting in a geometric evolution. In the computational subspace $\mathcal{S}_c$, the evolution operator is (omitting a global phase Θ_s)

$$U_T = \begin{pmatrix}\cos\Theta_s + i\sin\Theta_s\cos\theta & i\sin\Theta_s\sin\theta e^{i\phi}\\ i\sin\Theta_s\sin\theta e^{-i\phi} & \cos\Theta_s - i\sin\Theta_s\cos\theta\end{pmatrix}.$$

This is a universal single-qubit gate.

In this case, the gate time is $T \sim 18/c_2^k\Omega_k^{\rm peak}$. In the USC regime we can assume $c_k^m \gtrsim 0.1$ and $\omega_c/2\pi \sim 5$ GHz [72,73], resulting in $T \gg 5$ ns, i.e., the gate time can be tens of nanoseconds. Choosing $T = 35$ ns, $g \simeq 0.8\omega_c$, and $\omega_c/2\pi = 6.25$ GHz [104], the pulses $\Omega_{0,(2,4)}$ are shown in Fig. 3(a). Note there that the peak values of the pulses are $\Omega_k^{\rm peak}/2\pi \sim 200$ MHz. These satisfy the condition $\omega_c, g \gg \Omega_k$.

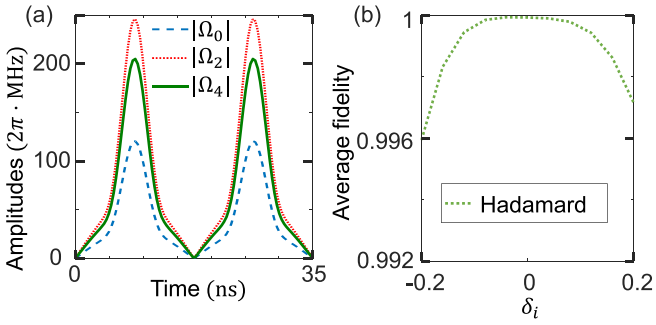

FIG. 3. For $(\Theta_s, \theta, \phi) = (\pi/2, \pi/4, 0)$, (i.e., the Hadamard gate): (a) finite-duration drives $\Omega_0 = (\Xi/\sqrt{2}c_0^2)\sin(\theta/2)$, $\Omega_2 = (\Xi/c_2^2)\cos(\theta/2)$, and $\Omega_4 = (\Xi/\sqrt{2}c_4^2)\sin(\theta/2)$ when $T = 35$ ns. (b) Average fidelity $\bar{F}$ of the Hadamard vs the error coefficient δ_i. The intermediate state is $|\zeta_2\rangle$ and the gate time is $T = 150$ ns. Other parameters are $g = 0.8\omega_c$ and $\omega_q = \omega_c = 2\pi \times 6.25$ GHz [104].

IV. ROBUSTNESS AGAINST CONTROL IMPERFECTIONS AND DECOHERENCE

It has been experimentally verified [110] that the pulses chosen based on β and φ in Eq. (19) can counteract the systematic errors induced by imperfections of the control fields Ω_k, making the computation insensitive to such errors [18,19,102]. In the presence of such imperfections with error parameter δ_i, the driving amplitudes become $\Omega_k^i = (1+\delta_i)\Omega_k$. Accordingly, the effective Hamiltonian $H_{\rm eff}(t)$ should be corrected as $H_{\rm eff}^i(t) = (1+\delta_i)H_{\rm eff}(t)$. By using time-dependent perturbation theory up to $\mathcal{O}(\delta_i)$, the evolution state of the system is approximatively

$$|\psi_-^i(t)\rangle \approx |\psi_-(t)\rangle - \frac{i\delta_i}{\hbar}\int_0^{t_f} U(t_f, t)H_{\rm eff}^i(t)|\psi_-(t)\rangle dt,$$

where $U(t_f, t)$ is the unperturbed time evolution operator.

We assume that the protocol works perfectly when $\delta_i = 0$, resulting in

$$P_{\text{out}} \approx 1 - \frac{\delta_i^2}{\hbar^2}\left|\int_0^{t_f} e^{2i\mathcal{R}_-(t)}\langle\psi_+(t)|H_{\text{eff}}(t)|\psi_-(t)\rangle dt\right|^2,$$

where P_{out} is the population of the output state after the gate operation, and

$$\mathcal{R}_-(t) = \frac{1}{\hbar}\int_0^t \langle\psi_-(t')|[i\hbar\partial_{t'} - H_{\text{eff}}(t')]|\psi_-(t')\rangle dt' \quad (20)$$

is the Lewis-Riesenfeld phase [99]. Then the systematic error sensitivity can be defined as [102]

$$q_i := -\frac{1}{2}\frac{\partial^2 P_{\text{out}}}{\partial\delta_i^2}\bigg|_{\delta_i=0} = \left|\int_0^{t_f} e^{i\beta+2i\mathcal{R}_-(t)}\dot{\varphi}\sin^2\varphi dt\right|^2. \quad (21)$$

Substituting φ and β [see Eq. (19)] into Eq. (21), we obtain $q_i \simeq 0$ [18,19,102], which means that the holonomic gates are insensitive to the systematic errors induced by the pulse imperfections.

The average fidelity of a gate over all possible initial states can be defined by [111,112]

$$\bar{F} = [\text{Tr}(MM^\dagger) + |\text{Tr}(M)|^2]/(D^2 + D), \quad (22)$$

with $M = \mathcal{P}_c U_T^\dagger U \mathcal{P}_c$. Here $\mathcal{P}_c$ (D) is the projector (dimension) of the subspace $\mathcal{S}_c$. The evolution operator U, describing the actual dynamical evolution, is calculated with the total Hamiltonian $H_{\text{tot}}(t) = H_0 + H_D(t)$. Using the above definition, in Fig. 3(b) we show the average fidelity $\bar{F}$ of the Hadamard gate versus the error coefficient δ_i. Note that when $\delta_i \in [-0.1, 0.1]$, the average fidelity is nearly 99.9%, indicating that our protocol is insensitive to the systematic error caused by pulse imperfections.

The average infidelities $(1 - \bar{F})$ of arbitrary single-qubit gates are shown in Fig. 4(a). The left (right) side of each circle denotes the average infidelity in the absence (presence) of pulse imperfections. When considering pulse imperfections with an error coefficient $\delta_i = 0.1$, the infidelities only slightly increase from $\sim 10^{-4}$ to $\sim 10^{-3}$. For instance, in the case of the Hadamard gate, pulse imperfections with an error coefficient $\delta_i = 0.1$ only increase the infidelity from $<10^{-4}$ to $\sim 10^{-3}$. This indicates that the generated gates are mostly insensitive to systematic errors.

Generally, a geometric gate can be robust against noise caused by amplitude fluctuations. Without loss of generality, we use additive white Gaussian noise to investigate the influence of such noise. In this case the driving amplitudes Ω_k should be corrected to be $\Omega_k^s = \text{AWGN}(\Omega_k, r)$. Here $\text{AWGN}(\Omega_k, r)$ is a function that generates the additive white Gaussian noise (AWGN) to the original signal Ω_k with a signal-to-noise ratio r. Because the additive white Gaussian noise is generated randomly in each single simulation, we perform the numerical simulation 20 times to estimate its average influence [see Fig. 4(b) with an illustration of the Hadamard gate]. As shown in Fig. 4(b), when considering relatively strong noises with $r = 15$, the gate fidelities can still

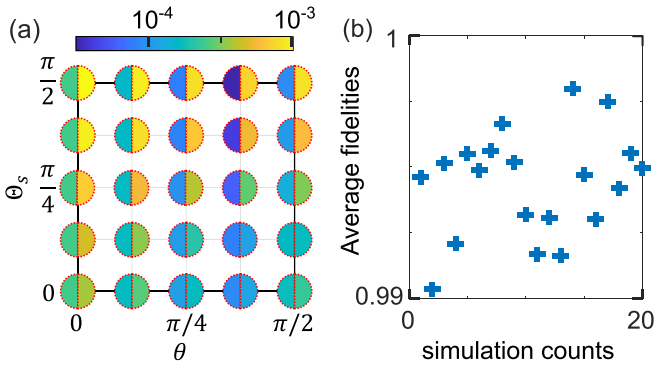

FIG. 4. (a) Average infidelities $(1 - \bar{F})$ of arbitrary single-qubit gates when $\phi = 0$ and $T = 150$ ns. Each circle denotes a single-qubit gate, e.g., $(\Theta_s, \theta) = (\pi/2, \pi/4)$ corresponds to the Hadamard gate. In each circle, the left (right) side denotes the infidelity in the absence (presence) of pulse imperfections. When considering pulse imperfections, the error coefficient is assumed to be $\delta_i = 0.1$. (b) Average fidelities $\bar{F}$ of the Hadamard gate vs simulation counts with an additive white Gaussian noise (AWGN). Each cross denotes the average gate fidelity when the signal-to-noise ratio is $r = 15$. Other parameters are the same as those in Fig. 3.

be higher than 99%. This indicates that our protocol is mostly insensitive to noise caused by amplitude fluctuations.

In the USC regime, relaxation and dephasing are studied in the basis $|\mathcal{E}_j\rangle$, which diagonalizes the Hamiltonian H_0. The master equation in the Born-Markov approximation, valid for generic hybrid-quantum systems, is [88–91,113]

$$\hbar\dot{\rho}(t) = i[\rho(t), H_{\text{tot}}(t)] + \sum_{\nu=0}^{3}\mathcal{D}\left[\sum_j \sqrt{\Lambda_\nu^{jj}}|\mathcal{E}_j\rangle\langle\mathcal{E}_j|\right]\rho(t) + \sum_{\nu'=0}^{5}\sum_{j>j',j'}\Gamma_{\nu'}^{jj'}\mathcal{D}[|\mathcal{E}_{j'}\rangle\langle\mathcal{E}_j|]\rho(t), \quad (23)$$

where $\mathcal{D}[\mathcal{O}]\rho(t) = \mathcal{O}\rho(t)\mathcal{O}^\dagger - [\rho(t)\mathcal{O}^\dagger\mathcal{O} + \mathcal{O}^\dagger\mathcal{O}\rho(t)]/2$ is the Lindblad superoperator. For simplicity, the dephasing and relaxation parameters have been written in a compact form:

$$\begin{aligned}
\Lambda_0^{jj} &= \kappa^\phi|\langle\mathcal{E}_j|a^\dagger a|\mathcal{E}_j\rangle|^2,\\
\Lambda_1^{jj} &= \kappa|\langle\mathcal{E}_j|a^\dagger + a|\mathcal{E}_j\rangle|^2,\\
\Lambda_{2,(3)}^{jj} &= \gamma_{g,(\mu)}^\phi|\langle\mathcal{E}_j|\sigma_{g,(\mu)}^z|\mathcal{E}_j\rangle|^2,\\
\Gamma_0^{jj'} &= \kappa^\phi|\langle\mathcal{E}_{j'}|a^\dagger a|\mathcal{E}_j\rangle|^2,\\
\Gamma_1^{jj'} &= \kappa|\langle\mathcal{E}_{j'}|a^\dagger + a|\mathcal{E}_j\rangle|^2,\\
\Gamma_{2,(3)}^{jj'} &= \gamma_{g,(\mu)}|\langle\mathcal{E}_{j'}|\sigma_{g,(\mu)}^x|\mathcal{E}_j\rangle|^2,\\
\Gamma_{4,(5)}^{jj'} &= \gamma_{g,(\mu)}^\phi|\langle\mathcal{E}_{j'}|\sigma_{g,(\mu)}^z|\mathcal{E}_j\rangle|^2.
\end{aligned} \quad (24)$$

Here $\sigma_\mu^x = |\mu\rangle\langle g| + |g\rangle\langle\mu|$, κ (κ^ϕ) is the cavity decay (dephasing) rate, $\gamma_{g,(\mu)}$ is the spontaneous emission rate of the transition $|e\rangle \to |g\rangle$ ($|g\rangle \to |\mu\rangle$), and $\gamma_{g,(\mu)}^\phi$ is the atomic dephasing rate corresponding to $\sigma_{g,(\mu)}^z$ ($\sigma_\mu^z = |g\rangle\langle g| - |\mu\rangle\langle\mu|$).

To check the robustness of the geometric gates against decoherence, we assume the input state as $|\psi_{\text{in}}\rangle = |\tilde{0}\rangle$, corresponding to an output state $|\psi_{\text{out}}\rangle = U_T|\psi_{\text{in}}\rangle$. Using

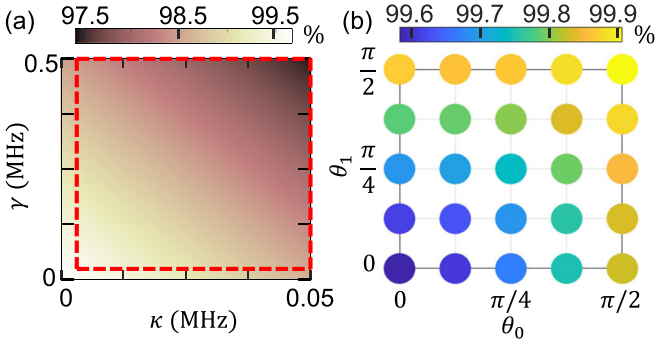

FIG. 5. (a) Fidelity F_{out} of the output state of the Hadamard gate vs κ and γ. The decay and dephasing rates in the red-dashed box have been achieved in experiments of superconducting circuits [53]. Other parameters are the same for Fig. 3. (b) Average fidelities of arbitrary two-qubit gates in the presence of pulse imperfections with an error coefficient $\delta_i = 0.1$. We assume $\Theta_s = \pi/2$ and $\phi = \pi$ for simplicity. Each circle denotes a two-qubit gate, e.g., $(\theta_0, \theta_1) = (0, \pi/2)$ corresponds to the controlled-NOT gate. The intermediate state is $|\zeta_0'\rangle$; parameters are $T = 750\,\text{ns}$, $g_a = g_b = 1.3\omega_c$, and $\omega_b = 0.9\omega_a$, $\omega_a = \omega_q = 2\pi \times 6.25\,\text{GHz}$.

$(\Theta_s, \theta, \phi) = (\pi/2, \pi/4, 0)$ (Hadamard gate), in Fig. 5(a) we show the fidelity $F_{\text{out}} = \langle\psi_{\text{out}}|\rho(t_f)|\psi_{\text{out}}\rangle$ versus γ and κ in the presence of pulse imperfections when $\delta_i = 0.1$. In this figure we notice that the dissipation and dephasing of the atom affect the evolution much weaker than those of the cavity. For experimentally realistic parameters of superconducting circuit experiments [55], $(\kappa, \kappa^{\phi}, \gamma_{g,(\mu)}, \gamma^{\phi}_{g,(\mu)}) \simeq 2\pi \times (0.33, 0.3, 8, 8)\,\text{kHz}$, the fidelity of the output state is $F_{\text{out}} \simeq 99.56\%$, indicating that our protocol is robust against decoherence.

V. MULTIQUBIT GATES

Our protocol can be extended to implement multiqubit holonomic gates, such as two-qubit gates. We consider that the Ξ-type atom ultrastrongly couples to a bimodal cavity (frequencies ω_a and ω_b). The system Hamiltonian is described by

$$H'_{\text{tot}} = H'_R + \hbar\omega_\mu|\mu\rangle\langle\mu| + H_D(t),$$
$$H'_R = \hbar\omega_a a^\dagger a + \hbar\omega_b b^\dagger b + \frac{\hbar\omega_q}{2}\sigma_g^z + \hbar[g_a(a + a^\dagger) + g_b(b + b^\dagger)]\sigma_g^x. \quad (25)$$

The eigenstates of H'_R corresponding to the eigenvalues E'_m can be described by

$$|\zeta'_m\rangle = \sum_{n_a,n_b,m} c^m_{n_a,n_b}|g\rangle|n_a\rangle_a|n_b\rangle_b + d^m_{n_a,n_b}|e\rangle|n_a\rangle_a|n_b\rangle_b, \quad (26)$$

where $|n_a\rangle_b$ and $|n_b\rangle_b$ denote the Fock states of the two cavity modes, respectively.

Then we assume that the driving field is

$$\Omega = \Omega_{k_a,k_b}\cos\left(\omega_{k_a,k_b} + \phi_{k_a,k_b}\right). \quad (27)$$

When choosing the frequencies that $\omega_a/\omega_b \neq 0, 1, 2\ldots$, and

$$\omega_{k_a,k_b} = E'_m - \omega_\mu - k_a\omega_a - k_b\omega_b, \quad (28)$$

the effective Hamiltonian is approximatively

$$H'_{\text{eff}}(t) = \frac{\hbar}{2}\sum_{k_a,k_b} c^m_{k_a,k_b}\Omega_{k_a,k_b}\exp(i\phi_{k_a,k_b})|\mu\rangle|k_a\rangle_a|k_b\rangle_b\langle\zeta'_m| + \text{H.c.}$$

For simplicity, we assume that the intermediate state is the dressed state $|\zeta'_0\rangle$, the driving amplitudes become

$$c^0_{0,0}\Omega_{0,0} = c^0_{0,4}\Omega^4_0 = c^0_{4,0}\Omega_{4,0} = c^0_{4,4}\Omega_{4,4} = \Xi_{\tilde{0}\tilde{0}}(t)/2,$$
$$c^0_{0,2}\Omega_{0,2} = c^0_{4,2}\Omega_{4,2} = \Xi_{\tilde{0}\tilde{1}}(t)/\sqrt{2},$$
$$c^0_{2,0}\Omega_{2,0} = c^0_{2,4}\Omega_{2,4} = \Xi_{\tilde{1}\tilde{0}}(t)/\sqrt{2},$$
$$c^0_{2,2}\Omega_{2,2} = \Xi_{\tilde{1}\tilde{1}}(t),$$

and the phases are

$$\phi_{0,0} = \phi_{0,4} = \phi_{4,0} = \phi_{4,4} = \phi_{\tilde{0}\tilde{0}},$$
$$\phi_{0,2} = \phi_{4,2} = \phi_{\tilde{0}\tilde{0}} + \phi,$$
$$\phi_{2,0} = \phi_{2,4} = \phi_{\tilde{0}\tilde{0}} + \phi,$$
$$\phi_{2,2} = \phi_{\tilde{0}\tilde{0}} + \phi. \quad (29)$$

Here, the auxiliary parameter $\phi_{\tilde{0}\tilde{0}}$ is time dependent and the auxiliary parameter ϕ is time independent.

The effective Hamiltonian in Eq. (29) becomes

$$\tilde{H}'_{\text{eff}}(t) = \frac{\hbar}{2}\Xi'_0(t)\exp[i\phi_{\tilde{0}\tilde{0}}]|\mu\rangle|b'\rangle\langle\zeta'_0| + \text{H.c.}, \quad (30)$$

with the binomial codes

$$|\tilde{0}\rangle_a = \frac{1}{\sqrt{2}}(|0\rangle_a + |4\rangle_a), \quad |\tilde{1}\rangle_a = |2\rangle_a,$$
$$|\tilde{0}\rangle_b = \frac{1}{\sqrt{2}}(|0\rangle_b + |4\rangle_b), \quad |\tilde{1}\rangle_b = |2\rangle_b. \quad (31)$$

Here, the bright state $|b'\rangle$ can be defined as

$$|b'\rangle = e^{-i\phi}\cos\frac{\theta_0}{2}\cos\frac{\theta_1}{2}|\tilde{0}\rangle_a|\tilde{0}\rangle_b + \cos\frac{\theta_0}{2}\sin\frac{\theta_1}{2}|\tilde{0}\rangle_a|\tilde{1}\rangle_b + \sin\frac{\theta_0}{2}\cos\frac{\theta_2}{2}|\tilde{1}\rangle_a|\tilde{0}\rangle_b + \sin\frac{\theta_0}{2}\sin\frac{\theta_2}{2}|\tilde{1}\rangle_a|\tilde{1}\rangle_b,$$

with auxiliary parameters

$$\Xi'_0(t) = \sqrt{[\Xi_{\tilde{0}\tilde{0}}(t)]^2 + [\Xi_{\tilde{0}\tilde{1}}(t)]^2 + [\Xi_{\tilde{1}\tilde{0}}(t)]^2 + [\Xi_{\tilde{1}\tilde{1}}(t)]^2},$$
$$\theta_0 = 2\arctan\left[\frac{\sqrt{\Xi^2_{\tilde{1}\tilde{0}}(t) + \Xi^2_{\tilde{1}\tilde{1}}(t)}}{\sqrt{\Xi^2_{\tilde{0}\tilde{0}}(t) + \Xi^2_{\tilde{0}\tilde{1}}(t)}}\right],$$
$$\theta_1 = 2\arctan\left[\frac{\Xi_{\tilde{0}\tilde{1}}(t)}{\Xi_{\tilde{0}\tilde{0}}(t)}\right], \quad \theta_2 = 2\arctan\left[\frac{\Xi_{\tilde{1}\tilde{1}}(t)}{\Xi_{\tilde{1}\tilde{0}}(t)}\right].$$

For simplicity, we choose $\theta_{0,(1,2)}$ to be time independent. The orthogonal partners of the state $|b'\rangle$ become

$$|d_1\rangle = e^{-i\phi}\sin\frac{\theta_0}{2}\cos\frac{\theta_1}{2}|\tilde{0}\rangle_a|\tilde{0}\rangle_b + \sin\frac{\theta_0}{2}\sin\frac{\theta_1}{2}|\tilde{0}\rangle_a|\tilde{1}\rangle_b - \cos\frac{\theta_0}{2}\cos\frac{\theta_2}{2}|\tilde{1}\rangle_a|\tilde{0}\rangle_b - \cos\frac{\theta_0}{2}\sin\frac{\theta_2}{2}|\tilde{1}\rangle_a|\tilde{1}\rangle_b,$$

TABLE I. Implementation examples of two-qubit gates.

Gate	Matrix	Parameters $(\Theta_s, \theta_0, \theta_1, \theta_2, \phi)$
CNOT	$\begin{pmatrix} 0 & 1 & 0 & 0 \\ 1 & 0 & 0 & 0 \\ 0 & 0 & 1 & 0 \\ 0 & 0 & 0 & 1 \end{pmatrix}$	$(\pi/2, 0, \pi/2, \pi/2, \pi)$
SWAP	$\begin{pmatrix} 1 & 0 & 0 & 0 \\ 0 & 0 & 1 & 0 \\ 0 & 1 & 0 & 0 \\ 0 & 0 & 0 & 1 \end{pmatrix}$	$(\pi/2, -\pi/2, 0, \pi, \pi)$
$\sqrt{\text{SWAP}}$	$\begin{pmatrix} 1 & 0 & 0 & 0 \\ 0 & \frac{1}{2}(1+i) & \frac{1}{2}(1-i) & 0 \\ 0 & \frac{1}{2}(1-i) & \frac{1}{2}(1+i) & 0 \\ 0 & 0 & 0 & 1 \end{pmatrix}$	$(\pi/4, -\pi/2, \pi, 0, \pi)$

$$
\begin{aligned}
|d_2\rangle &= e^{-i\phi}\cos\frac{\theta_0}{2}\sin\frac{\theta_1}{2}|\tilde{0}\rangle_a|\tilde{0}\rangle_b - \cos\frac{\theta_0}{2}\cos\frac{\theta_1}{2}|\tilde{0}\rangle_a|\tilde{1}\rangle_b \\
&\quad + \sin\frac{\theta_0}{2}\sin\frac{\theta_2}{2}|\tilde{1}\rangle_a|\tilde{0}\rangle_b - \sin\frac{\theta_0}{2}\cos\frac{\theta_2}{2}|\tilde{1}\rangle_a|\tilde{1}\rangle_b, \\
|d_3\rangle &= e^{-i\phi}\sin\frac{\theta_0}{2}\sin\frac{\theta_1}{2}|\tilde{0}\rangle_a|\tilde{0}\rangle_b - \sin\frac{\theta_0}{2}\cos\frac{\theta_1}{2}|\tilde{0}\rangle_a|\tilde{1}\rangle_b \\
&\quad - \cos\frac{\theta_0}{2}\sin\frac{\theta_2}{2}|\tilde{1}\rangle_a|\tilde{0}\rangle_b + \cos\frac{\theta_0}{2}\cos\frac{\theta_2}{2}|\tilde{1}\rangle_a|\tilde{1}\rangle_b.
\end{aligned}
$$

Then, by using the same strategy as that of the single-qubit case, we choose

$$
\begin{aligned}
\Xi'_0(t)\sin\phi_{\tilde{0}\tilde{0}} &= \Omega_p(\beta,\varphi)/2 = \dot{\beta}\cot\varphi\sin\beta + \dot{\varphi}\cos\beta, \\
\Xi'_0(t)\cos\phi_{\tilde{0}\tilde{0}} &= \Omega_s(\beta',\varphi)/2 = \dot{\beta}\cot\varphi\cos\beta - \dot{\varphi}\sin\beta.
\end{aligned}
$$

The evolution operator after a cyclic evolution along

$$
|\psi'_-(t)\rangle = ie^{i\beta}(\varphi/2)|\mu\rangle|b\rangle + \sin(\varphi/2)|\zeta'_0\rangle \tag{32}
$$

in the subspace spanned by $\{|b'\rangle, |d_1\rangle, |d_2\rangle, |d_3\rangle\}$ is given by

$$
U'_T = \begin{pmatrix} \exp(2i\Theta_s) & 0 & 0 & 0 \\ 0 & 1 & 0 & 0 \\ 0 & 0 & 1 & 0 \\ 0 & 0 & 0 & 1 \end{pmatrix}. \tag{33}
$$

In the computational subspace spanned by $\{|\tilde{0}\rangle_a|\tilde{0}\rangle_b, |\tilde{0}\rangle_a|\tilde{1}\rangle_b, |\tilde{1}\rangle_a|\tilde{0}\rangle_b, |\tilde{1}\rangle_a|\tilde{1}\rangle_b\}$, the evolution operator U'_T describes a universal two-qubit geometric gate (see Table I for examples). These two-qubit gates using the same strategy as the single-qubit case are also insensitive to the errors induced by pulse imperfections. Therefore, when considering the error coefficient $\delta_i = 0.1$, in Fig. 5(b) we show that arbitrary two-qubit gates can be implemented with high fidelities.

VI. PREPARING SUPERPOSITIONS OF FOCK STATES

High-fidelity input states are needed to verify the feasibility of the proposed NHQC in experiments. To generate these input states, starting from Eq. (6), we assume

$$
\begin{aligned}
&\phi_0 = 0, \quad c^m_{k'}\Omega_{k'} = \epsilon_{k'}\Omega_s(\tilde{\beta},\tilde{\varphi}), \\
&\phi_{k'} = \pi, \quad c^m_0\Omega_0 = \Omega_p(\tilde{\beta},\tilde{\varphi}),
\end{aligned} \tag{34}
$$

where $k' \neq 0$ are even numbers, $\epsilon_{k'}$ are time-independent coefficients satisfying $\sum_{k'}|\epsilon_{k'}|^2 = 1$, $\tilde{\beta}$, and $\tilde{\varphi}$ satisfying $\tilde{\beta}(0) \simeq \tilde{\varphi}(0) \simeq 0$ are time-dependent auxiliary parameters to be determined. Then the evolution governed by $H_{\text{eff}}(t)$ is

$$
\begin{aligned}
|\tilde{\psi}_0(t)\rangle &= \cos\tilde{\varphi}(\cos\tilde{\beta}|0\rangle + \sin\tilde{\beta}\sum_{k'}\epsilon_{k'}|k'\rangle)|\mu\rangle \\
&\quad - i\sin\tilde{\varphi}|\zeta_2\rangle.
\end{aligned} \tag{35}
$$

When $\tilde{\varphi}(t_f) \simeq 0$ and $\tilde{\beta}(t_f) = \tilde{\beta}_f$, we obtain

$$
|\tilde{\psi}_0(t_f)\rangle = \left(\cos\tilde{\beta}_f|0\rangle + \sin\tilde{\beta}_f\sum_{k'}\epsilon_{k'}|k'\rangle\right)|\mu\rangle, \tag{36}
$$

which is an arbitrary superposition of even-number Fock states. The boundaries for $\tilde{\beta}$ and $\tilde{\varphi}$ can be satisfied by choosing

$$
\begin{aligned}
\tilde{\beta} &= \frac{\tilde{\beta}_f}{[1+\exp(-t/\tau + T/2\tau)]}, \\
\tilde{\varphi} &= \frac{\tilde{\varphi}_0}{\exp(t/\tau_c - T/2\tau_c)^2},
\end{aligned} \tag{37}
$$

with parameters $(\tilde{\varphi}_0, \tau, \tau_c) = (\pi/5, 0.115T, 0.3T)$ [114,115].

For instance, when $k = (0, 2, 4)$, $m = 2$, $\tilde{\beta}_f = \arccos(1/\sqrt{6})$, and $\epsilon_2 = 2/\sqrt{5}$ we can generate an input state $|\psi_{\text{in}}\rangle = (|\tilde{0}\rangle + \sqrt{2}|\tilde{1}\rangle)/\sqrt{3}$, as shown in Fig. 6(a). This figure shows the final populations $P_k = \langle\mu|\langle k|\rho(t_f)|k\rangle|\mu\rangle$ and the Wigner function $W(\alpha) = 2\text{Tr}[D^\dagger_\alpha\rho(t_f)D_\alpha e^{i\pi a^\dagger a}]/\pi$, where $D_\alpha = \exp(\alpha a^\dagger - \alpha^* a)$ is the displacement operator. As shown in Fig. 6(a) the full dynamics [green histograms] is in excellent agreement with the effective dynamics [yellow histograms].

In the presence of decoherence, the populations [red-solid broken line in Fig. 6(a)], calculated using the master equation in Eq. (23), are almost the same as those calculated using the coherent dynamics when feasible parameters are considered. This indicates that our protocol for the state preparations is robust against decoherence.

The above approach can be used to generate Schrödinger's cat states [116–121], e.g., the even cat state

$$
\left|\mathcal{C}^\eta_e\right\rangle = e^{|\eta|^2/2}\sqrt{\text{sech}|\eta|^2}(|\eta\rangle + |-\eta\rangle)/2, \tag{38}
$$

when $m = 0$, $\tilde{\beta}_f = \arccos(\sqrt{\text{sech}|\eta|^2})$, and $\epsilon_{k'} = -(\eta^{k'}\cot\tilde{\beta}_f)/\sqrt{k'!}$, where η is the amplitude of the coherent state $|\eta\rangle$. In Fig. 6(b), we show that the even cat state can be generated with a high fidelity. These generated high-fidelity cat stats are useful for cat-code quantum computation [48,51].

VII. CONCLUSION

We have investigated the possibility of using USC systems for the implementation of *fast, robust, and fault-tolerant* holonomic computation. The dressed-state properties of the USC systems allow one to *simultaneously couple* the dressed state

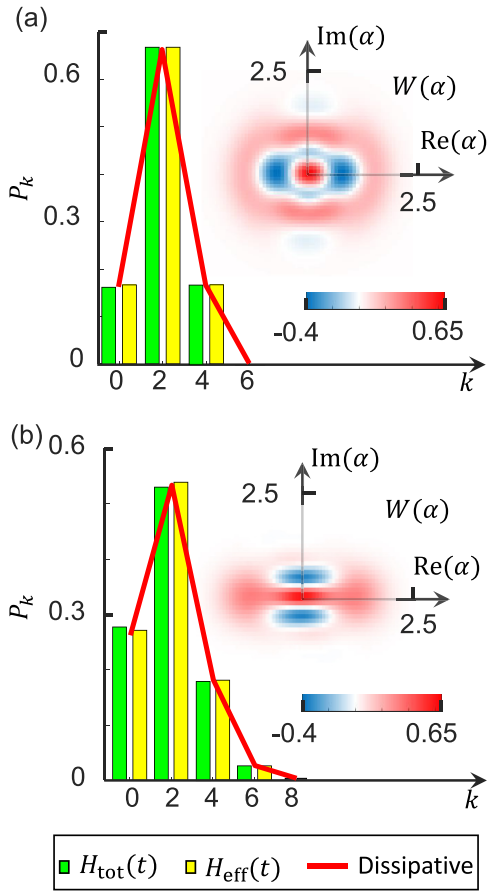

FIG. 6. Histograms of Fock-state populations calculated with the total Hamiltonian $H_{\rm tot}(t)$ (green) and the effective Hamiltonian $H_{\rm eff}(t)$ (yellow). The red-solid broken lines in each panel denote the Fock-state population calculated by the master equation in Eq. (23) when $(\kappa, \kappa^{\phi}, \gamma_{g,(\mu)}, \gamma^{\phi}_{g,(\mu)}) \simeq 2\pi \times (0.33, 0.3, 8, 8)$ kHz [55]. Insets show the Wigner function $W(\alpha)$ of the generated states. (a) The superposition state $|\psi_{\rm in}\rangle = (|\tilde{0}\rangle + \sqrt{2}|\tilde{1}\rangle)/\sqrt{3}$ with parameters $\tilde{\beta}_f = \arccos(\sqrt{1/6})$, $\epsilon_2 = 2/\sqrt{5}$, and $g = 0.7\omega_c$. (b) The cat state $|\mathcal{C}^{\eta}_{e}\rangle$ with amplitude $\eta = g/\omega_c = \sqrt{2}$. The evolution time for each panel is $T = 35$ ns.

$|\zeta_m\rangle$ to multiple Fock sates, such that one can manipulate the population and the phase of each Fock state as desired. The binomial codes formed from these Fock states are protected against the single-photon loss, making the computation fault tolerant. Moreover, by designing the pulses with invariant-based engineering, we can eliminate the dynamical phase and achieve only the geometric phase in a cyclic evolution. Such a control technique is compatible with the systematic-error-sensitivity nullification method, making the evolution mostly insensitive to the systematic errors caused by pulse imperfections. Additionally, using the USC regime allows one to apply relatively strong driving fields, such that our protocols are fast. As a result, our protocols are robust against the decays and dephasings of the cavity and the atom. Note that this work can freely control a bosonic mode. The proposed idea can be generalized to realize NHQC with other bosonic error-correction qubits, such as cat qubits [48,51], for fast, robust, and fault-tolerant quantum computation.

TABLE II. Superconducting experiments that have achieved the ultrastrong light-matter coupling. Abbreviations are FQ=flux qubit, TR=transmon qubit, TL=transmission-line resonator, and LE=lumped-element resonator.

Year & Ref.	Qubit	Cavity	$g/2\pi$ (MHz)	$\omega_c/2\pi$ (GHz)	g/ω_c
2010 [129]	FQ	TL	636	5.357	0.12
2010 [130]	FQ	LE	810	8.13	0.1
2017 [104]	FQ	LE	7630	5.711	1.34
2017 [135]	FQ	LE	5310	6.203	0.86
2017 [131]	TR	TL	897	4.268	0.19
2018 [136]	FQ	LE	7480	6.335	1.18

The proposed protocols can be realized in superconducting circuits [72,73,104,122–136]. For instance, one can inductively couple a flux qubit and an *LC* oscillator via Josephson junctions [104] to reach the needed coupling strength. The quantized level structure in Fig. 1(b) can be realized adjusting the external magnetic flux through the qubit loop [89–91].

Some experimental observations of the ultrastrong light-matter coupling in superconducting quantum circuits are listed in Table II. To reach the ultrastrong and deep-strong coupling regimes, we can choose a setup with a flux qubit coupled to a lumped-element *LC* resonator [104,135]. In such superconducting circuit experiments, qubit and resonator frequencies are usually in the range $\omega_{c,(q)}/2\pi \sim 1$–$10$ GHz. Thus we choose $g/\omega_c \simeq 0.7\,(0.8)$ and $\omega_c/2\pi = 6.25$ GHz, which are experimentally feasible, as shown in Table II.

Recent experimental work has demonstrated that dissipation and dephasing rates in a flux qubit is of the order of $2\pi \times 10$ kHz [73,137,138]. The transmon qubits, which have lower anharmonicity than flux qubits, can have dissipation and dephasing rates approaching $2\pi \times 1$ kHz [139,140]. For transmission-line resonators, quality factors factors $Q = \omega_c/\kappa$ on the order of 10^6 have been realized [141], which indicates that quantum coherence of single photons up to $1 \sim 10$ ms is within current experimental capabilities [142]. Therefore our proposal works well in the USC regime, and it may find compelling applications for quantum information processing for various USC systems, in particular, superconducting systems.

ACKNOWLEDGMENTS

We acknowledge helpful discussions with Y.-H. Kang and Z.-B. Yang. Y.-H.C. is supported by the Japan Society for the Promotion of Science (JSPS) KAKENHI through Grant No. JP19F19028. X.W. is supported by the China Postdoctoral Science Foundation through Grant No. 2018M631136 and the Natural Science Foundation of China under Grant No. 11804270. F.N. is supported in part by the Nippon Telegraph and Telephone Corporation (NTT) Research, the Japan Science and Technology Agency (JST) [via the Quantum Leap Flagship Program (Q-LEAP), Moonshot R&D Grant No. JPMJMS2061, and the Centers of Research Excellence in Science and Technology (CREST) Grant No. JPMJCR1676], the Japan Society for the Promotion of Science (JSPS) [via Grants-in-Aid for Scientific Research (KAKENHI) Grant No. JP20H00134 and JSPS-RFBR Grant No. JPJSBP120194828],

the Army Research Office (ARO) (Grant No. W911NF-18-1-0358), the Asian Office of Aerospace Research and Development (AOARD) (via Grant No. FA2386-20-1-4069), and the Foundational Questions Institute Fund (FQXi) (via Grant No. FQXi-IAF19-06).

APPENDIX A: EFFECTIVE HAMILTONIAN

The total Hamiltonian for this protocol can be written as

$$H_{\rm tot} = H_0 + H_D(t),$$
$$H_0 = \hbar\sum_{m=0}^{\infty} E_m|\zeta_m\rangle\langle\zeta_m| + \sum_{n=0}^{\infty}\hbar(\omega_\mu + n\omega_c)|\mu\rangle\langle\mu|\otimes|n\rangle\langle n|,$$
$$H_D(t) = \hbar\Omega(|\mu\rangle\langle g| + |g\rangle\langle\mu|). \tag{A1}$$

Here $|\zeta_m\rangle$ are the dressed eigenstates of the Rabi Hamiltonian with eigenvalues E_m, ω_μ denotes the energy of the lowest atomic level $|\mu\rangle$, n is the cavity photon number, and $\Omega = \Omega_k\cos(\omega_k t + \phi_k)$ is a composite pulse driving the atomic transition $|\mu\rangle \leftrightarrow |g\rangle$. Performing the unitary transformation $U_d = \exp(-iH_0 t/\hbar)$ and choosing the frequencies as $\omega_k = E_m - \omega_\mu - k\omega_c$, we have

$$\begin{aligned} H_D'(t) = \frac{\hbar}{2}\sum_k\sum_{m'}\sum_n c_n^{m'}\Omega_k|\mu\rangle|n\rangle\langle\zeta_{m'}| \\ \times\{\exp[-i\Delta E_{m,m'}t + i(n-k)\omega_c t + i\phi_k] \\ + \exp[-i\Delta E_{m,m'}t + i(n-k)\omega_c t - 2i\omega_k t - i\phi_k]\} \\ + \text{H.c.}, \end{aligned} \tag{A2}$$

where $\Delta E_{m,m'} = E_{m'} - E_m$ is the energy gap between the eigenstates $|\zeta_{m'}\rangle$ and $|\zeta_m\rangle$.

Obviously, when satisfying

$$\begin{aligned} c_n^{m'}\Omega_k &\ll |(n-k)\omega_c - \Delta E_{m,m'}|, \\ c_n^{m'}\Omega_k &\ll |(n-k)\omega_c - 2\omega_k - \Delta E_{m,m'}|, \end{aligned} \tag{A3}$$

the fast-oscillating terms can be neglected in the rotating wave approximation (RWA). Then, the effective Hamiltonian becomes

$$H_{\rm eff}(t) = \frac{\hbar}{2}\sum_k c_k^m\Omega_k e^{i\phi_k}|\mu\rangle|k\rangle\langle\zeta_m| + \text{H.c.}, \tag{A4}$$

i.e., the effective Hamiltonian in Eq. (6). The coefficients $c_n^m = \langle\zeta_m|g\rangle|n\rangle$ and $d_{n\pm1}^m = \langle\zeta_m|e\rangle|n\pm1\rangle$ can be obtained numerically [see Fig. 7(a) as an example for the ground dressed state $|\zeta_0\rangle$]. According to our numerical results, when $0.5 \lesssim g/\omega_c \lesssim 1$, the probability amplitudes (c_0^2, c_2^2, c_4^2) of the states $(|g\rangle|0\rangle, |g\rangle|2\rangle, |g\rangle|4\rangle)$ in the third dressed state $|\zeta_2\rangle$ are greater [see Fig. 7(b)] than in the others. Thus, when focusing on manipulating the Fock states $(|0\rangle, |2\rangle, |4\rangle)$, the effective driving intensities (i.e., $c_0^2\Omega_0$, $c_2^2\Omega_2$, and $c_4^2\Omega_4$) can be much stronger by using $|\zeta_2\rangle$ to be the intermediate state. Therefore the gate time can be shortened. In Fig. 7(b), we find that the coefficients c_n^m jump from zero to nonzero values when $g/\omega_c \simeq 0.43$. This is caused by an avoided level crossing [72,73] when $g/\omega_c \simeq 0.43$ [see the red circle in Fig. 7(c)]. In Fig. 7(c) we notice that the dressed states become nonequidistant as the energy gap $\Delta E_{m,m+1} \neq$ constant when $0.1 \lesssim g/\omega_c \lesssim 1$. For instance, when $g/\omega_c \sim 0.5$, we have $|\Delta E_{m,m+1} - \Delta E_{m+1,m+2}| \gtrsim 0.5\omega_c$. This indicates that the USC can induce strong anharmonicity in the dressed states $|\zeta_m\rangle$.

APPENDIX B: DYNAMICAL AND GEOMETRIC PHASES

An operator $I(t)$ satisfying $\hbar\partial_t I(t) = i[H(t), I(t)]$ is a dynamical invariant of an arbitrary Hamiltonian $H(t)$. According to [99], an arbitrary solution of the Schrödinger equation,

$$i\hbar\frac{\partial}{\partial t}|\psi(t)\rangle = H(t)|\psi(t)\rangle, \tag{B1}$$

can be expressed by using the eigenstates of $I(t)$ as

$$\begin{aligned} |\psi(t)\rangle &= \sum_n C_n e^{i\mathcal{R}_n(t)}|\psi_n(t)\rangle, \\ \mathcal{R}_n(t) &= \frac{1}{\hbar}\int_0^t\langle\psi_n(t')|[i\hbar\partial_{t'} - H(t')]|\psi_n(t')\rangle dt', \end{aligned} \tag{B2}$$

where C_n are time-independent amplitudes, $|\psi_n(t)\rangle$ are the orthonormal eigenvectors of $I(t)$, and $\mathcal{R}_n(t)$ are the Lewis-Riesenfeld phases [99]. These phases include dynamical phases

$$\vartheta_n(t) = -\frac{1}{\hbar}\int_0^t\langle\psi_n(t')|H(t')|\psi_n(t')\rangle dt' \tag{B3}$$

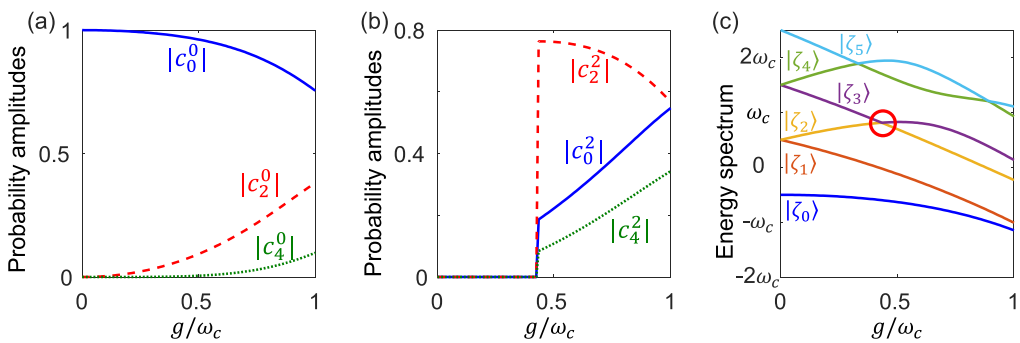

FIG. 7. Probability amplitudes of $|g\rangle|0\rangle$, $|g\rangle|2\rangle$, and $|g\rangle|4\rangle$ in dressed states (a) $|\zeta_0\rangle$ and (b) $|\zeta_2\rangle$ of H_R as a function of the coupling strength g when $\omega_q = \omega_c$. (c) Energy spectrum of the Hamiltonian H_R when $\omega_q = \omega_c$. The red circle in panel (c) denotes an avoided level crossing.

and geometric phases

$$\Theta_n(t) = \int_0^t \langle\psi_n(t')|i\partial_{t'}|\psi_n(t')\rangle dt'. \tag{B4}$$

For instance, when $\langle\psi(0)|\psi_0(0)\rangle = 1$, we have $C_0 = 1$ and $C_{n\neq 0} = 0$. The evolution of the system is exactly along the eigenstate $|\psi_0(t)\rangle$, which is a shortcut to the adiabatic passage of $H(t)$.

The effective Hamiltonian,

$$H_{\text{eff}}(t) = \frac{\hbar}{2}\Omega_0 e^{i\phi_2}|\zeta_2\rangle\langle b|\langle\mu| + \text{H.c.}, \tag{B5}$$

in Eq. (13) for the NHQC can be regarded as the intermediate state $|\zeta_2\rangle$ coupled to the bright state

$$|b\rangle = e^{-i\phi}\sin(\theta/2)|\tilde{0}\rangle + \cos(\theta/2)|\tilde{1}\rangle \tag{B6}$$

but decoupled from the dark state

$$|d\rangle = e^{-i\phi}\cos(\theta/2)|\tilde{1}\rangle - \sin(\theta/2)|\tilde{0}\rangle. \tag{B7}$$

A dynamical invariant of $H_{\text{eff}}(t)$ is

$$\begin{aligned} I(t) = {} & \cos\varphi(|\zeta_2\rangle\langle\zeta_2| - |b\rangle\langle b|\otimes|\mu\rangle\langle\mu|) \\ & + (e^{i\beta}\sin\varphi|\zeta_2\rangle\langle b|\langle\mu| + \text{H.c.}) \end{aligned} \tag{B8}$$

with eigenvectors

$$\begin{aligned} |\psi_+(t)\rangle &= \sin(\varphi/2)|\mu\rangle|b\rangle + ie^{-i\beta}\cos(\varphi/2)|\zeta_2\rangle, \\ |\psi_-(t)\rangle &= ie^{i\beta}\cos(\varphi/2)|\mu\rangle|b\rangle + \sin(\varphi/2)|\zeta_2\rangle. \end{aligned} \tag{B9}$$

Then, substituting Eqs. (B5) and (B9), into Eq. (B2), the time derivatives of the dynamic phases and geometric phases acquired by $|\psi_\pm(t)\rangle$ are

$$\begin{aligned} \dot{\vartheta}_\pm(t) &= \mp\frac{\dot{\beta}}{2}\sin\varphi\tan\varphi, \\ \dot{\Theta}_\pm(t) &= \pm\frac{\dot{\beta}}{2}(1-\cos\varphi), \end{aligned} \tag{B10}$$

respectively. Obviously, $\dot{\vartheta}_\pm(t)$ and $\dot{\Theta}_\pm(t)$ obey the same mathematical symmetry. To eliminate the dynamical phases and achieve only the geometric phases, we can design a piecewise function for β, e.g.,

$$\beta = \begin{cases} f(t), & t\in[0, t_f/2] \\ f(t) - 2\Theta_s, & t\in[t_f/2, t_f] \end{cases}, \tag{B11}$$

where Θ_s is a constant. Then we assume $\dot{\vartheta}_\pm(t - t_f/2)$ to be odd functions, leading to

$$\begin{aligned} \vartheta_\pm &= \mp\int_{\frac{t_f}{2}}^{\frac{t_f}{2}+\Delta t}\Theta_s(\sin\varphi\tan\varphi)dt + \int_0^{t_f}\dot{\vartheta}_\pm(t)dt \\ &= \mp\Theta_s\sin\varphi\left(\frac{t_f}{2}\right)\tan\varphi\left(\frac{t_f}{2}\right). \end{aligned} \tag{B12}$$

Here, Δt is a small increase in time, and we have assumed φ to be continuous in time. Meanwhile, for the geometric phases, $\dot{\Theta}_\pm(t - t_f/2)$ are also odd functions, leading to

$$\begin{aligned} \Theta_\pm &= \mp\int_{\frac{t_f}{2}}^{\frac{t_f}{2}+\Delta t}\Theta_s(1-\cos\varphi)dt + \int_0^{t_f}\dot{\Theta}_\pm(t)dt \\ &= \mp\Theta_s\left[1 - \cos\varphi\left(\frac{t_f}{2}\right)\right]. \end{aligned} \tag{B13}$$

Thus, we obtain $\vartheta_\pm = 0$ and $\Theta_\pm = \mp 2\Theta_s$ when $\varphi(t_f/2) = \pi$.

[1] P. Zanardi and M. Rasetti, Holonomic quantum computation, Phys. Lett. A **264**, 94 (1999).

[2] S.-L. Zhu and Z. D. Wang, Implementation of Universal Quantum Gates Based on Nonadiabatic Geometric Phases, Phys. Rev. Lett. **89**, 097902 (2002).

[3] E. Sjöqvist, D. M. Tong, L. M. Andersson, B. Hessmo, M. Johansson, and K. Singh, Non-adiabatic holonomic quantum computation, New J. Phys. **14**, 103035 (2012).

[4] G. F. Xu, J. Zhang, D. M. Tong, E. Sjöqvist, and L. C. Kwek, Nonadiabatic Holonomic Quantum Computation in Decoherence-Free Subspaces, Phys. Rev. Lett. **109**, 170501 (2012).

[5] M. V. Berry, Quantal phase factors accompanying adiabatic changes, Proc. R. Soc. London, Ser. A **392**, 45 (1984).

[6] Y. Aharonov and J. Anandan, Phase Change During a Cyclic Quantum Evolution, Phys. Rev. Lett. **58**, 1593 (1987).

[7] J. Anandan, Non-adiabatic non-Abelian geometric phase, Phys. Lett. A **133**, 171 (1988).

[8] F. Wilczek and A. Zee, Appearance of Gauge Structure in Simple Dynamical Systems, Phys. Rev. Lett. **52**, 2111 (1984).

[9] L.-A. Wu, P. Zanardi, and D. A. Lidar, Holonomic Quantum Computation in Decoherence-Free Subspaces, Phys. Rev. Lett. **95**, 130501 (2005).

[10] P. Solinas, P. Zanardi, and N. Zanghì, Robustness of non-Abelian holonomic quantum gates against parametric noise, Phys. Rev. A **70**, 042316 (2004).

[11] S.-L. Zhu and P. Zanardi, Geometric quantum gates that are robust against stochastic control errors, Phys. Rev. A **72**, 020301(R) (2005).

[12] P. Solinas, M. Sassetti, P. Truini, and N. Zanghì, On the stability of quantum holonomic gates, New J. Phys. **14**, 093006 (2012).

[13] M. Johansson, E. Sjöqvist, L. M. Andersson, M. Ericsson, B. Hessmo, K. Singh, and D. M. Tong, Robustness of nonadiabatic holonomic gates, Phys. Rev. A **86**, 062322 (2012).

[14] Q.-X. Lv, Z.-T. Liang, H.-Z. Liu, J.-H. Liang, K.-Y. Liao, and Y.-X. Du, Noncyclic geometric quantum computation with shortcut to adiabaticity, Phys. Rev. A **101**, 022330 (2020).

[15] Y.-X. Du, X.-X. Yue, Z.-T. Liang, J.-Z. Li, H. Yan, and S.-L. Zhu, Geometric atom interferometry with shortcuts to adiabaticity, Phys. Rev. A **95**, 043608 (2017).

[16] Z.-T. Liang, X. Yue, Q. Lv, Y.-X. Du, W. Huang, H. Yan, and S.-L. Zhu, Proposal for implementing universal superadiabatic geometric quantum gates in nitrogen-vacancy centers, Phys. Rev. A **93**, 040305(R) (2016).

[17] B.-J. Liu, X.-K. Song, Z.-Y. Xue, X. Wang, and M.-H. Yung, Plug-and-Play Approach to Nonadiabatic Geometric Quantum Gates, Phys. Rev. Lett. **123**, 100501 (2019).

[18] Y.-H. Kang, Z.-C. Shi, B.-H. Huang, J. Song, and Y. Xia, Flexible scheme for the implementation of nonadiabatic geometric quantum computation, Phys. Rev. A **101**, 032322 (2020).

[19] D. Daems, A. Ruschhaupt, D. Sugny, and S. Guérin, Robust Quantum Control by a Single-Shot Shaped Pulse, Phys. Rev. Lett. **111**, 050404 (2013).

[20] T. Chen, P. Shen, and Z.-Y. Xue, Robust and Fast Holonomic Quantum Gates with Encoding on Superconducting Circuits, Phys. Rev. Appl. **14**, 034038 (2020).

[21] O. Oreshkov, T. A. Brun, and D. A. Lidar, Fault-Tolerant Holonomic Quantum Computation, Phys. Rev. Lett. **102**, 070502 (2009).

[22] T. Chen and Z.-Y. Xue, Nonadiabatic Geometric Quantum Computation with Parametrically Tunable Coupling, Phys. Rev. Appl. **10**, 054051 (2018).

[23] C. Wu, Y. Wang, X.-L. Feng, and J.-L. Chen, Holonomic Quantum Computation in Surface Codes, Phys. Rev. Appl. **13**, 014055 (2020).

[24] J. Zhang, S. J. Devitt, J. Q. You, and F. Nori, Holonomic surface codes for fault-tolerant quantum computation, Phys. Rev. A **97**, 022335 (2018).

[25] A. G. Fowler, M. Mariantoni, J. M. Martinis, and A. N. Cleland, Surface codes: Towards practical large-scale quantum computation, Phys. Rev. A **86**, 032324 (2012).

[26] S. Li and Z.-Y. Xue, Dynamically corrected nonadiabatic holonomic quantum gates, arXiv:2012.09034.

[27] J. M. Martinis, Qubit metrology for building a fault-tolerant quantum computer, npj Quantum Inf. **1**, 15005 (2015).

[28] J. Chiaverini, D. Leibfried, T. Schaetz, M. D. Barrett, R. B. Blakestad, J. Britton, W. M. Itano, J. D. Jost, E. Knill, C. Langer, R. Ozeri, and D. J. Wineland, Realization of quantum error correction, Nature (London) **432**, 602 (2004).

[29] P. Schindler, J. T. Barreiro, T. Monz, V. Nebendahl, D. Nigg, M. Chwalla, M. Hennrich, and R. Blatt, Experimental repetitive quantum error correction, Science **332**, 1059 (2011).

[30] J. Kelly, R. Barends, A. G. Fowler, A. Megrant, E. Jeffrey, T. C. White, D. Sank, J. Y. Mutus, B. Campbell, Y. Chen, Z. Chen, B. Chiaro, A. Dunsworth, I.-C. Hoi, C. Neill, P. J. J. O'Malley, C. Quintana, P. Roushan, A. Vainsencher, J. Wenner *et al.*, State preservation by repetitive error detection in a superconducting quantum circuit, Nature (London) **519**, 66 (2015).

[31] G. Waldherr, Y. Wang, S. Zaiser, M. Jamali, T. Schulte-Herbrüggen, H. Abe, T. Ohshima, J. Isoya, J. F. Du, P. Neumann, and J. Wrachtrup, Quantum error correction in a solid-state hybrid spin register, Nature (London) **506**, 204 (2014).

[32] J. Zhang, L.-C. Kwek, Erik Sjöqvist, D. M. Tong, and P. Zanardi, Quantum computation in noiseless subsystems with fast non-Abelian holonomies, Phys. Rev. A **89**, 042302 (2014).

[33] B.-J. Liu, Z.-H. Huang, Z.-Y. Xue, and X.-D. Zhang, Superadiabatic holonomic quantum computation in cavity QED, Phys. Rev. A **95**, 062308 (2017).

[34] Z.-Y. Xue, F.-L. Gu, Z.-P. Hong, Z.-H. Yang, D.-W. Zhang, Y. Hu, and J. Q. You, Nonadiabatic Holonomic Quantum Computation with Dressed-State Qubits, Phys. Rev. Appl. **7**, 054022 (2017).

[35] A. A. Abdumalikov, Jr., J. M. Fink, K. Juliusson, M. Pechal, S. Berger, A. Wallraff, and S. Filipp, Experimental realization of non-Abelian non-adiabatic geometric gates, Nature (London) **496**, 482 (2013).

[36] G. Feng, G. Xu, and G. Long, Experimental Realization of Nonadiabatic Holonomic Quantum Computation, Phys. Rev. Lett. **110**, 190501 (2013).

[37] Z. Zhu, T. Chen, X. Yang, J. Bian, Z.-Y. Xue, and X. Peng, Single-Loop and Composite-Loop Realization of Nonadiabatic Holonomic Quantum Gates in a Decoherence-Free Subspace, Phys. Rev. Appl. **12**, 024024 (2019).

[38] C. Zu, W.-B. Wang, L. He, W.-G. Zhang, C.-Y. Dai, F. Wang, and L.-M. Duan, Experimental realization of universal geometric quantum gates with solid-state spins, Nature (London) **514**, 72 (2014).

[39] Y. Sekiguchi, N. Niikura, R. Kuroiwa, H. Kano, and H. Kosaka, Optical holonomic single quantum gates with a geometric spin under a zero field, Nat. Photon. **11**, 309 (2017).

[40] Y. Xu, W. Cai, Y. Ma, X. Mu, L. Hu, T. Chen, H. Wang, Y. P. Song, Z.-Y. Xue, Z.-Q. Yin, and L. Sun, Single-Loop Realization of Arbitrary Nonadiabatic Holonomic Single-Qubit Quantum Gates in a Superconducting Circuit, Phys. Rev. Lett. **121**, 110501 (2018).

[41] Y. Wang, Y. Su, X. Chen, and C. Wu, Dephasing-Protected Scalable Holonomic Quantum Computation on a Rabi Lattice, Phys. Rev. Appl. **14**, 044043 (2020).

[42] Y. Xu, Z. Hua, T. Chen, X. Pan, X. Li, J. Han, W. Cai, Y. Ma, H. Wang, Y. P. Song, Z.-Y. Xue, and L. Sun, Experimental Implementation of Universal Nonadiabatic Geometric Quantum Gates in a Superconducting Circuit, Phys. Rev. Lett. **124**, 230503 (2020).

[43] D. Gottesman, An introduction to quantum error correction and fault-tolerant quantum computation, arXiv:0904.2557.

[44] P. W. Shor, Scheme for reducing decoherence in quantum computer memory, Phys. Rev. A **52**, R2493 (1995).

[45] A. Steane, Multiple-particle interference and quantum error correction, Proc. R. Soc. London, Ser. A **452**, 2551 (1996).

[46] I. L. Chuang, D. W. Leung, and Y. Yamamoto, Bosonic quantum codes for amplitude damping, Phys. Rev. A **56**, 1114 (1997).

[47] D. Gottesman, A. Kitaev, and J. Preskill, Encoding a qubit in an oscillator, Phys. Rev. A **64**, 012310 (2001).

[48] V. V. Albert, C. Shu, S. Krastanov, C. Shen, R.-B. Liu, Z.-B. Yang, R. J. Schoelkopf, M. Mirrahimi, M. H. Devoret, and L. Jiang, Holonomic Quantum Control with Continuous Variable Systems, Phys. Rev. Lett. **116**, 140502 (2016).

[49] V. V. Albert, S. O. Mundhada, A. G. S. Touzard, M. H. Devoret, and L. Jiang, Pair-cat codes: Autonomous error-correction with low-order nonlinearity, Quantum Sci. Technol. **4**, 035007 (2019).

[50] V. V. Albert, K. Noh, K. Duivenvoorden, D. J. Young, R. T. Brierley, P. Reinhold, C. Vuillot, L. Li, C. Shen, S. M. Girvin, B. M. Terhal, and L. Jiang, Performance and structure of single-mode bosonic codes, Phys. Rev. A **97**, 032346 (2018).

[51] M. Mirrahimi, Z. Leghtas, V. V. Albert, S. Touzard, R. J. Schoelkopf, L. Jiang, and M. H. Devoret, Dynamically protected cat-qubits: A new paradigm for universal quantum computation, New J. Phys. **16**, 045014 (2014).

[52] L. Li, C.-L. Zou, V. V. Albert, S. Muralidharan, S. M. Girvin, and L. Jiang, Cat Codes with Optimal Decoherence

Suppression for a Lossy Bosonic Channel, Phys. Rev. Lett. **119**, 030502 (2017).

[53] W. Cai, Y. Ma, W. Wang, C.-L. Zou, and L. Sun, Bosonic quantum error correction codes in superconducting quantum circuits, Fundam. Res. **1**, 50 (2021).

[54] M. H. Michael, M. Silveri, R. T. Brierley, V. V. Albert, J. Salmilehto, L. Jiang, and S. M. Girvin, New Class of Quantum Error-Correcting Codes for a Bosonic Mode, Phys. Rev. X **6**, 031006 (2016).

[55] Y. Xu, Y. Ma, W. Cai, X. Mu, W. Dai, W. Wang, L. Hu, X. Li, J. Han, H. Wang, Y. P. Song, Z.-B. Yang, S.-B. Zheng, and L. Sun, Demonstration of Controlled-Phase Gates between Two Error-Correctable Photonic Qubits, Phys. Rev. Lett. **124**, 120501 (2020).

[56] R. W. Heeres, P. Reinhold, N. Ofek, L. Frunzio, L. Jiang, M. H. Devoret, and R. J. Schoelkopf, Implementing a universal gate set on a logical qubit encoded in an oscillator, Nat. Commun. **8**, 94 (2017).

[57] S. Zhou, M. Zhang, J. Preskill, and L. Jiang, Achieving the Heisenberg limit in quantum metrology using quantum error correction, Nat. Commun. **9**, 78 (2018).

[58] C. J. Axline, L. D. Burkhart, W. Pfaff, M. Zhang, K. Chou, P. Campagne-Ibarcq, P. Reinhold, L. Frunzio, S. M. Girvin, L. Jiang, M. H. Devoret, and R. J. Schoelkopf, On-demand quantum state transfer and entanglement between remote microwave cavity memories, Nat. Phys. **14**, 705 (2018).

[59] K. S. Chou, J. Z. Blumoff, C. S. Wang, P. C. Reinhold, C. J. Axline, Y. Y. Gao, L. Frunzio, M. H. Devoret, L. Jiang, and R. J. Schoelkopf, Deterministic teleportation of a quantum gate between two logical qubits, Nature (London) **561**, 368 (2018).

[60] L. Hu, Y. Ma, W. Cai, X. Mu, Y. Xu, W. Wang, Y. Wu, H. Wang, Y. P. Song, C.-L. Zou, S. M. Girvin, L-M. Duan, and L. Sun, Quantum error correction and universal gate set operation on a binomial bosonic logical qubit, Nat. Phys. **15**, 503 (2019).

[61] B. Vlastakis, G. Kirchmair, Z. Leghtas, S. E. Nigg, L. Frunzio, S. M. Girvin, M. Mirrahimi, M. H. Devoret, and R. J. Schoelkopf, Deterministically encoding quantum information using 100-photon Schrödinger cat states, Science **342**, 607 (2013).

[62] Z. Leghtas, S. Touzard, I. M. Pop, A. Kou, B. Vlastakis, A. Petrenko, K. M. Sliwa, A. Narla, S. Shankar, M. J. Hatridge, M. Reagor, L. Frunzio, R. J. Schoelkopf, M. Mirrahimi, and M. H. Devoret, Confining the state of light to a quantum manifold by engineered two-photon loss, Science **347**, 853 (2015).

[63] S. Rosenblum, Y. Y. Gao, P. Reinhold, C. Wang, C. J. Axline, L. Frunzio, S. M. Girvin, L. Jiang, M. Mirrahimi, M. H. Devoret *et al.*, A CNOT gate between multiphoton qubits encoded in two cavities, Nat. Commun. **9**, 652 (2018).

[64] A. Grimm, N. E. Frattini, S. Puri, S. O. Mundhada, S. Touzard, M. Mirrahimi, S. M. Girvin, S. Shankar, and M. H. Devoret, Stabilization and operation of a Kerr-cat qubit, Nature (London) **584**, 205 (2020).

[65] N. Ofek, A. Petrenko, R. Heeres, P. Reinhold, Z. Leghtas, B. Vlastakis, Y. Liu, L. Frunzio, S. M. Girvin, L. Jiang, Ma. Mirrahimi, M. H. Devoret, and R. J. Schoelkopf, Extending the lifetime of a quantum bit with error correction in superconducting circuits, Nature (London) **536**, 441 (2016).

[66] P. Campagne-Ibarcq, A. Eickbusch, S. Touzard, E. Zalys-Geller, N. E. Frattini, V. V. Sivak, P. Reinhold, S. Puri, S. Shankar, R. J. Schoelkopf, L. Frunzio, M. Mirrahimi, and M. H. Devoret, Quantum error correction of a qubit encoded in grid states of an oscillator, Nature (London) **584**, 368 (2020).

[67] S. Krastanov, V. V. Albert, C. Shen, C.-L. Zou, R. W. Heeres, B. Vlastakis, R. J. Schoelkopf, and L. Jiang, Universal control of an oscillator with dispersive coupling to a qubit, Phys. Rev. A **92**, 040303(R) (2015).

[68] R. W. Heeres, B. Vlastakis, E. Holland, S. Krastanov, V. V. Albert, L. Frunzio, L. Jiang, and R. J. Schoelkopf, Cavity State Manipulation using Photon-Number Selective Phase Gates, Phys. Rev. Lett. **115**, 137002 (2015).

[69] M. Amniat-Talab, S. Guérin, and H. R. Jauslin, Quantum averaging and resonances: Two-level atom in a one-mode quantized field, J. Math. Phys. **46**, 042311 (2005).

[70] E. K. Irish, Generalized Rotating-Wave Approximation for Arbitrarily Large Coupling, Phys. Rev. Lett. **99**, 173601 (2007).

[71] D. Braak, Integrability of the Rabi Model, Phys. Rev. Lett. **107**, 100401 (2011).

[72] A. F. Kockum, A. Miranowicz, S. De Liberato, S. Savasta, and F. Nori, Ultrastrong coupling between light and matter, Nat. Rev. Phys. **1**, 19 (2019).

[73] P. Forn-Díaz, L. Lamata, E. Rico, J. Kono, and E. Solano, Ultrastrong coupling regimes of light-matter interaction, Rev. Mod. Phys. **91**, 025005 (2019).

[74] C. J. Gan and H. Zheng, Dynamics of a two-level system coupled to a quantum oscillator: Transformed rotating-wave approximation, Eur. Phys. J. D **59**, 473 (2010).

[75] S. De Liberato, C. Ciuti, and I. Carusotto, Quantum Vacuum Radiation Spectra from a Semiconductor Microcavity with a Time-Modulated Vacuum Rabi Frequency, Phys. Rev. Lett. **98**, 103602 (2007).

[76] S. Ashhab and F. Nori, Qubit-oscillator systems in the ultrastrong-coupling regime and their potential for preparing nonclassical states, Phys. Rev. A **81**, 042311 (2010).

[77] S. De Liberato, Light-Matter Decoupling in the Deep Strong Coupling Regime: The Breakdown of the Purcell Effect, Phys. Rev. Lett. **112**, 016401 (2014).

[78] J. Casanova, G. Romero, I. Lizuain, J. J. García-Ripoll, and E. Solano, Deep Strong Coupling Regime of the Jaynes-Cummings Model, Phys. Rev. Lett. **105**, 263603 (2010).

[79] L. Garziano, V. Macrì, R. Stassi, O. Di Stefano, F. Nori, and S. Savasta, One Photon can Simultaneously Excite Two or More Atoms, Phys. Rev. Lett. **117**, 043601 (2016).

[80] X. Wang, A. Miranowicz, H.-R. Li, and F. Nori, Observing pure effects of counter-rotating terms without ultrastrong coupling: A single photon can simultaneously excite two qubits, Phys. Rev. A **96**, 063820 (2017).

[81] V. Macrì, F. Nori, and A. F. Kockum, Simple preparation of Bell and Greenberger-Horne-Zeilinger states using ultrastrong-coupling circuit QED, Phys. Rev. A **98**, 062327 (2018).

[82] O. Di Stefano, A. Settineri, V. Macrì, L. Garziano, R. Stassi, S. Savasta, and F. Nori, Resolution of gauge ambiguities in ultrastrong-coupling cavity quantum electrodynamics, Nat. Phys. **15**, 803 (2019).

[83] D. Z. Rossatto, C. J. Villas-Bôas, M. Sanz, and E. Solano, Spectral classification of coupling regimes in

the quantum Rabi model, Phys. Rev. A **96**, 013849 (2017).

[84] X. Cao, J. Q. You, H. Zheng, A. G. Kofman, and F. Nori, Dynamics and quantum Zeno effect for a qubit in either a low- or high-frequency bath beyond the rotating-wave approximation, Phys. Rev. A **82**, 022119 (2010).

[85] M. Cirio, S. De Liberato, N. Lambert, and F. Nori, Ground State Electroluminescence, Phys. Rev. Lett. **116**, 113601 (2016).

[86] M. Cirio, K. Debnath, N. Lambert, and F. Nori, Amplified Optomechanical Transduction of Virtual Radiation Pressure, Phys. Rev. Lett. **119**, 053601 (2017).

[87] M. Cirio, N. Shammah, N. Lambert, S. De Liberato, and F. Nori, Multielectron Ground State Electroluminescence, Phys. Rev. Lett. **122**, 190403 (2019).

[88] F. Beaudoin, J. M. Gambetta, and A. Blais, Dissipation and ultrastrong coupling in circuit QED, Phys. Rev. A **84**, 043832 (2011).

[89] R. Stassi, A. Ridolfo, O. Di Stefano, M. J. Hartmann, and S. Savasta, Spontaneous Conversion from Virtual to Real Photons in the Ultrastrong-Coupling Regime, Phys. Rev. Lett. **110**, 243601 (2013).

[90] O. Di Stefano, R. Stassi, L. Garziano, A. F. Kockum, S. Savasta, and F. Nori, Feynman-diagrams approach to the quantum Rabi model for ultrastrong cavity QED: Stimulated emission and reabsorption of virtual particles dressing a physical excitation, New J. Phys. **19**, 053010 (2017).

[91] J.-F. Huang and C. K. Law, Photon emission via vacuum-dressed intermediate states under ultrastrong coupling, Phys. Rev. A **89**, 033827 (2014).

[92] Y. Wang, J. Zhang, C. Wu, J. Q. You, and G. Romero, Holonomic quantum computation in the ultrastrong-coupling regime of circuit QED, Phys. Rev. A **94**, 012328 (2016).

[93] R. Stassi, M. Cirio, and F. Nori, Scalable quantum computer with superconducting circuits in the ultrastrong coupling regime, npj Quan. Inf. **6**, 67 (2020).

[94] H. Mukai, A. Tomonaga, and J.-S. Tsai, Superconducting quantum annealing architecture with LC resonators, J. Phys. Soc. Jpn. **88**, 061011 (2019).

[95] D. Guéry-Odelin, A. Ruschhaupt, A. Kiely, E. Torrontegui, S. Martínez-Garaot, and J. G. Muga, Shortcuts to adiabaticity: Concepts, methods, and applications, Rev. Mod. Phys. **91**, 045001 (2019).

[96] E. Torrontegui, S. Ibáñez, S. Martínez-Garaot, M. Modugno, A. del Campo, D. Guéry-Odelin, A. Ruschhaupt, X. Chen, and J. G. Muga, Shortcuts to adiabaticity, Adv. At. Mol. Opt. Phys. **62**, 117 (2013).

[97] A. Baksic, H. Ribeiro, and A. A. Clerk, Speeding up Adiabatic Quantum State Transfer by Using Dressed States, Phys. Rev. Lett. **116**, 230503 (2016).

[98] Y.-H. Chen, W. Qin, X. Wang, A. Miranowicz, and F. Nori, Shortcuts to Adiabaticity for the Quantum Rabi Model: Efficient Generation of Giant Entangled cat States via Parametric Amplification, Phys. Rev. Lett. **126**, 023602 (2021).

[99] H. R. Lewis and W. B. Riesenfeld, An exact quantum theory of the time-dependent harmonic oscillator and of a charged particle in a time-dependent electromagnetic field, J. Math. Phys. **10**, 1458 (1969).

[100] X. Chen and J. G. Muga, Engineering of fast population transfer in three-level systems, Phys. Rev. A **86**, 033405 (2012).

[101] Y.-H. Chen, Y. Xia, Q.-Q. Chen, and J. Song, Efficient shortcuts to adiabatic passage for fast population transfer in multiparticle systems, Phys. Rev. A **89**, 033856 (2014).

[102] A. Ruschhaupt, X. Chen, D. Alonso, and J. G. Muga, Optimally robust shortcuts to population inversion in two-level quantum systems, New J. Phys. **14**, 093040 (2012).

[103] R. Stassi, A. Ridolfo, S. Savasta, R. Girlanda, and O. Di Stefano, Delayed-choice quantum control of light-matter interaction, Europhys. Lett. **99**, 24003 (2012).

[104] F. Yoshihara, T. Fuse, S. Ashhab, K. Kakuyanagi, S. Saito, and K. Semba, Superconducting qubit–oscillator circuit beyond the ultrastrong-coupling regime, Nat. Phys. **13**, 44 (2016).

[105] W. Wang, L. Hu, Y. Xu, K. Liu, Y. Ma, S.-B. Zheng, R. Vijay, Y. P. Song, L.-M. Duan, and L. Sun, Converting Quasiclassical States Into Arbitrary Fock State Superpositions in a Superconducting Circuit, Phys. Rev. Lett. **118**, 223604 (2017).

[106] A. Vepsäläinen, S. Danilin, and G. S. Paraoanu, Superadiabatic population transfer in a three-level superconducting circuit, Sci. Adv. **5**, eaau5999 (2019).

[107] C. H. Bennett, D. P. DiVincenzo, J. A. Smolin, and W. K. Wootters, Mixed-state entanglement and quantum error correction, Phys. Rev. A **54**, 3824 (1996).

[108] E. Knill and R. Laflamme, Theory of quantum error-correcting codes, Phys. Rev. A **55**, 900 (1997).

[109] X. Chen, E. Torrontegui, and J. G. Muga, Lewis-Riesenfeld invariants and transitionless quantum driving, Phys. Rev. A **83**, 062116 (2011).

[110] M.-Z. Ai, S. Li, Z. Hou, R. He, Z.-H. Qian, Z.-Y. Xue, J.-M. Cui, Y.-F. Huang, C.-F. Li, and G.-C. Guo, Experimental Realization of Nonadiabatic Holonomic Single-Qubit Quantum Gates with Optimal Control in a Trapped Ion, Phys. Rev. Appl. **14**, 054062 (2020).

[111] P. Zanardi and D. A. Lidar, Purity and state fidelity of quantum channels, Phys. Rev. A **70**, 012315 (2004).

[112] L. H. Pedersen, N. M. Møller, and K. Mølmer, Fidelity of quantum operations, Phys. Lett. A **367**, 47 (2007).

[113] R. Stassi and F. Nori, Long-lasting quantum memories: Extending the coherence time of superconducting artificial atoms in the ultrastrong-coupling regime, Phys. Rev. A **97**, 033823 (2018).

[114] G. S. Vasilev, A. Kuhn, and N. V. Vitanov, Optimum pulse shapes for stimulated Raman adiabatic passage, Phys. Rev. A **80**, 013417 (2009).

[115] K. Bergmann, H. Theuer, and B. W. Shore, Coherent population transfer among quantum states of atoms and molecules, Rev. Mod. Phys. **70**, 1003 (1998).

[116] V. V. Dodonov, I. A. Malkin, and V. I. Man'ko, Even and odd coherent states and excitations of a singular oscillator, Physica **72**, 597 (1974).

[117] Y.-X. Liu, L. F. Wei, and F. Nori, Preparation of macroscopic quantum superposition states of a cavity field via coupling to a superconducting charge qubit, Phys. Rev. A **71**, 063820 (2005).

[118] M. Kira, S. W. Koch, R. P. Smith, A. E. Hunter, and S. T. Cundiff, Quantum spectroscopy with Schrödinger-cat states, Nat. Phys. **7**, 799 (2011).

[119] W. F. Braasch, O. D. Friedman, A. J. Rimberg, and M. P. Blencowe, Wigner current for open quantum systems, Phys. Rev. A **100**, 012124 (2019).

[120] Z.-Y. Zhou, C. Gneiting, J. Q. You, and F. Nori, Generating and detecting entangled cat states in dissipatively coupled degenerate optical parametric oscillators, Phys. Rev. A **104**, 013715 (2021).

[121] W. Qin, A. Miranowicz, H. Jing, and F. Nori, Generating Long-Lived Macroscopically Distinct Superposition States in Atomic Ensembles, Phys. Rev. Lett. **127**, 093602 (2021).

[122] P. D. Nation, J. R. Johansson, M. P. Blencowe, and F. Nori, Colloquium: Stimulating uncertainty: Amplifying the quantum vacuum with superconducting circuits, Rev. Mod. Phys. **84**, 1 (2012).

[123] Z. L. Xiang, S. Ashhab, J. Q. You, and F. Nori, Hybrid quantum circuits: Superconducting circuits interacting with other quantum systems, Rev. Mod. Phys. **85**, 623 (2013).

[124] X. Gu, A. F. Kockum, A. Miranowicz, Y.-X. Liu, and F. Nori, Microwave photonics with superconducting quantum circuits, Phys. Rep. **718-719**, 1 (2017).

[125] J. Q. You and F. Nori, Atomic physics and quantum optics using superconducting circuits, Nature (London) **474**, 589 (2011).

[126] M. H. Devoret, S. Girvin, and R. Schoelkopf, Circuit-QED: How strong can the coupling between a Josephson junction atom and a transmission line resonator be? Ann. Phys. **16**, 767 (2007).

[127] J. R. Johansson, G. Johansson, and F. Nori, Optomechanical-like coupling between superconducting resonators, Phys. Rev. A **90**, 053833 (2014).

[128] J. R. Johansson, G. Johansson, C. M. Wilson, and F. Nori, Dynamical Casimir Effect in a Superconducting Coplanar Waveguide, Phys. Rev. Lett. **103**, 147003 (2009).

[129] T. Niemczyk, F. Deppe, H. Huebl, E. P. Menzel, F. Hocke, M. J. Schwarz, J. J. Garcia-Ripoll, D. Zueco, T. Hümmer, E. Solano, A. Marx, and R. Gross, Circuit quantum electrodynamics in the ultrastrong-coupling regime, Nat. Phys. **6**, 772 (2010).

[130] P. Forn-Díaz, J. Lisenfeld, D. Marcos, J. J. García-Ripoll, E. Solano, C. J. P. M. Harmans, and J. E. Mooij, Observation of the Bloch-Siegert Shift in a Qubit-Oscillator System in the Ultrastrong Coupling Regime, Phys. Rev. Lett. **105**, 237001 (2010).

[131] S. J. Bosman, M. F. Gely, V. Singh, A. Bruno, D. Bothner, and G. A. Steele, Multi-mode ultra-strong coupling in circuit quantum electrodynamics, npj Quantum Inf. **3**, 46 (2017).

[132] P. Forn-Díaz, G. Romero, C. J. P. M. Harmans, E. Solano, and J. E. Mooij, Broken selection rule in the quantum Rabi model, Sci. Rep. **6**, 26720 (2016).

[133] A. Baust, E. Hoffmann, M. Haeberlein, M. J. Schwarz, P. Eder, J. Goetz, F. Wulschner, E. Xie, L. Zhong, F. Quijandria, D. Zueco, J. J. Ripoll, L. Garcia-Alvarez, G. Romero, E. Solano, K. G. Fedorov, E. P. Menzel, F. Deppe, A. Marx, and R. Gross, Ultrastrong coupling in two-resonator circuit QED, Phys. Rev. B **93**, 214501(R) (2016).

[134] Z. Chen, Y. Wang, T. Li, L. Tian, Y. Qiu, K. Inomata, F. Yoshihara, S. Han, F. Nori, J. S. Tsai, and J. Q. You, Single-photon-driven high-order sideband transitions in an ultrastrongly coupled circuit-quantum-electrodynamics system, Phys. Rev. A **96**, 012325 (2017).

[135] F. Yoshihara, T. Fuse, S. Ashhab, K. Kakuyanagi, S. Saito, and K. Semba, Characteristic spectra of circuit quantum electrodynamics systems from the ultrastrong- to the deep-strong-coupling regime, Phys. Rev. A **95**, 053824 (2017).

[136] F. Yoshihara, T. Fuse, Z. Ao, S. Ashhab, K. Kakuyanagi, S. Saito, T. Aoki, K. Koshino, and K. Semba, Inversion of Qubit Energy Levels in Qubit-Oscillator Circuits in the Deep-Strong-Coupling Regime, Phys. Rev. Lett. **120**, 183601 (2018).

[137] M. Stern, G. Catelani, Y. Kubo, C. Grezes, A. Bienfait, D. Vion, D. Esteve, and P. Bertet, Flux Qubits with Long Coherence Times for Hybrid Quantum Circuits, Phys. Rev. Lett. **113**, 123601 (2014).

[138] J.-L. Orgiazzi, C. Deng, D. Layden, R. Marchildon, F. Kitapli, F. Shen, M. Bal, F. R. Ong, and A. Lupascu, Flux qubits in a planar circuit quantum electrodynamics architecture: Quantum control and decoherence, Phys. Rev. B **93**, 104518 (2016).

[139] J. Q. You, X. Hu, S. Ashhab, and F. Nori, Low-decoherence flux qubit, Phys. Rev. B **75**, 140515(R) (2007).

[140] F. Yan, S. Gustavsson, A. Kamal, J.y Birenbaum, A. P. Sears, D. Hover, T. J. Gudmundsen, D. Rosenberg, G. Samach, S. Weber, J. L. Yoder, T. P. Orlando, J. Clarke, A. J. Kerman, and W. D. Oliver, The flux qubit revisited to enhance coherence and reproducibility, Nat. Commun. **7**, 12964 (2016).

[141] H. Paik, D. I. Schuster, L. S. Bishop, G. Kirchmair, G. Catelani, A. P. Sears, B. R. Johnson, M. J. Reagor, L. Frunzio, L. I. Glazman, S. M. Girvin, M. H. Devoret, and R. J. Schoelkopf, Observation of High Coherence in Josephson Junction Qubits Measured in a Three-Dimensional Circuit QED Architecture, Phys. Rev. Lett. **107**, 240501 (2011).

[142] A. Megrant, C. Neill, R. Barends, B. Chiaro, Y. Chen, L. Feigl, J. Kelly, E. Lucero, M. Mariantoni, P. J. J. O'Malley, D. Sank, A. Vainsencher, J. Wenner, T. C. White, Y. Yin, J. Zhao, C. J. Palmstrøm, J. M. Martinis, and A. N. Cleland, Planar superconducting resonators with internal quality factors above one million, Appl. Phys. Lett. **100**, 113510 (2012).